MRI thermometry in phantoms by use of the proton resonance frequency shift method: application to interstitial laser thermotherapy

Olsrud, Johan; Wirestam, Ronnie; Brockstedt, Sara; Nilsson, Annika M K; Tranberg, Karl-Göran; Ståhlberg, Freddy; Persson, Bertil R

Published in:
Physics in Medicine and Biology

1998

MRI thermometry in phantoms by use of the proton resonance frequency shift method: application to interstitial laser thermotherapy

1998 Phys. Med. Biol. 43 2597

(http://iopscience.iop.org/0031-9155/43/9/012)

Phys. Med. Biol. **43** (1998) 2597–2613. Printed in the UK PII: S0031-9155(98)90137-3

MRI thermometry in phantoms by use of the proton resonance frequency shift method: application to interstitial laser thermotherapy

Johan Olsrud†, Ronnie Wirestam†, Sara Brockstedt†, Annika M K Nilsson‖, Karl-Göran Tranberg§, Freddy Ståhlberg†‡ and Bertil R R Persson†

† Department of Radiation Physics, Lund University Hospital, SE-221 85 Lund, Sweden
‡ Department of Diagnostic Radiology, Lund University Hospital, SE-221 85 Lund, Sweden
§ Department of Surgery, Lund University Hospital, SE-221 85 Lund, Sweden
‖ Department of Physics, Lund Institute of Technology, SE-221 00 Lund, Sweden

Received 15 December 1997, in final form 17 April 1998

Abstract. In this work the temperature dependence of the proton resonance frequency was assessed in agarose gel with a high melting temperature (95 °C) and in porcine liver *in vitro* at temperatures relevant to thermotherapy (25–80 °C). Furthermore, an optically tissue-like agarose gel phantom was developed and evaluated for use in MRI. The phantom was used to visualize temperature distributions from a diffusing laser fibre by means of the proton resonance frequency shift mehod. An approximately linear relationship (0.0085 ppm $^{\circ}C^{-1}$) between proton resonance frequency shift and temperature change was found for agarose gel, whereas deviations from a linear relationship were observed for porcine liver. The optically tissue-like agarose gel allowed reliable MRI temperature monitoring, and the MR relaxation times (T_1 and T_2) and the optical properties were found to be independently alterable. Temperature distributions around a diffusing laser fibre, during irradiation and subsequent cooling, were assessed with high spatial resolution (voxel size = 4.3 mm^3) and with random uncertainties ranging from 0.3 °C to 1.4 °C (1 SD) with a 40 s scan time.

1. Introduction

Non-invasive temperature monitoring is important for the development of hyperthermia and thermotherapy (Cetas and Connor 1978, Bolomey and Hawley 1990), and magnetic resonance imaging (MRI) seems to be a promising method. Three main parameters, the spin–lattice relaxation time (T_1), the molecular diffusion coefficient and the proton resonance frequency, have been examined with respect to their temperature dependence (LeBihan 1995, Jolesz and Zientara 1995).

Consequently, MRI has been proposed as a non-invasive temperature monitoring method for interstitial laser thermotherapy (ILT) (Jolesz *et al* 1988, Jolesz and Zientara 1995). ILT is a method for local heating of malignant tumours (Bown *et al* 1983), causing cells to be irreversibly damaged depending on temperature and time. The heat is delivered using one or several optical fibres that emit laser light which is eventually absorbed in the surrounding tissue. The temperature distribution, and thus the treated volume, depends on the laser power, irradiation time and on the characteristics and positions of the optical fibres. The treated volume also depends on the optical and thermal properties of the tissue as well as on the blood flow (McKenzie 1990, Möller *et al* 1997, Sturesson 1998). With a thorough

0031-9155/98/092597+17$19.50

knowledge about the characteristics of the ILT system and the optical and thermal properties of the tissue, 'thermal dose planning' may be performed by solving the bioheat equation using numerical methods (Sturesson and Andersson-Engels 1995, Roggan and Müller 1995, Ivarsson *et al* 1998). However, the fibre positions and the accuracy of the calculations need to be verified during treatments. MR thermal imaging, which is non-invasive and volumetric in its nature, as opposed to thermistors or thermocouples which are invasive and provide point measurements only, might well serve this purpose. Furthermore, accurate non-invasive volumetric temperature monitoring in phantoms would be helpful to characterize laser fibres and to verify numerical calculations, as proposed by Hushek *et al* (1993) and Clegg *et al* (1995).

Among the various MRI methods, the proton resonance frequency shift (PRF) method has been shown to be the most accurate in phantoms (De Poorter *et al* 1994). The temperature dependence of the proton resonance frequency has recently been examined in materials such as gels (agarose or polyacrylamide) and tissue *in vitro* (Kuroda *et al* 1991, De Poorter *et al* 1994, Ishihara *et al* 1995, Cline *et al* 1996, Jakob *et al* 1997, Vitkin *et al* 1997, Harth *et al* 1997), usually at temperatures below $\sim 55\,^{\circ}$C. Optically tissue-like liquid phantoms have sometimes been used for optical experiments. The optical properties may be altered by addition of scattering and absorbing agents, such as polystyrene microspheres and India ink or molecular dyes (Marijnissen and Star 1984, Madsen *et al* 1992, Nilsson *et al* 1995). Solid phantoms based on an epoxy resin and silica spheres have been developed by Firbank *et al* (1995) and Sukowski *et al* (1996). Gel phantoms that are optically tissue-like were recently reported by Hushek *et al* (1993) and Wagnières *et al* (1997). Hushek *et al* used polyacrylamide phantoms for MRI temperature monitoring. Agarose gels, as used in this study, with tissue-like optical properties have not previously been used for such applications.

In this work, the PRF method was elucidated as a temperature monitoring tool for ILT phantom measurements. The temperature dependence of the proton resonance frequency was examined in a temperature range relevant to thermotherapy (25–80 °C), both in agarose gel and in tissue *in vitro*. Agarose gel with various concentrations of scattering and absorbing agents was evaluated as an optically tissue-like phantom material for use in MRI. The accuracy and precision of the PRF method, when used to depict the temperature distributions from a diffusing laser fibre in the gel phantom, was assessed.

2. Theory

The local magnetic field (magnetic flux density), B_{loc}, experienced by a proton within an object is related to the main magnetic field of the MRI scanner, B_0, according to

$$B_{\mathrm{loc}} = (1 - \sigma_{\mathrm{tot}})B_0 + \delta B_0$$

where σ_{tot} is the total screening constant of the proton and δB_0 represents local deviations from B_0 that are not temperature dependent. When the temperature increases, the total screening constant increases (linearly) which causes B_{loc} to decrease (Schneider *et al* 1958, Hindman 1966). A gradient echo pulse sequence may be used to obtain phase distribution images with high spatial and temporal resolution. Subtraction of two phase images of the same volume (slice), obtained at different times, will reveal temperature changes between image acquisitions (Ishihara *et al* 1995, De Poorter *et al* 1994). According to the Larmor equation, the phase (in radians) measured within a voxel at a temperature T is given by

$$\varphi(T) = \gamma T_E[(1 - \sigma_{\mathrm{tot}}(T))B_0 + \delta B_0]$$

where γ is the gyromagnetic ratio of hydrogen ($\gamma/2\pi = 42.577 \times 10^6$ s^{-1} T^{-1}) and T_E is the echo time of the gradient echo pulse sequence. If a second image is acquired when the temperature within the same voxel has changed to T', a different phase will be measured. Subtraction of the first image from the second image results in a phase difference within the voxel according to

$$\Delta\varphi = \varphi(T') - \varphi(T) = \gamma T_E(\sigma_{\text{tot}}(T) - \sigma_{\text{tot}}(T'))B_0 = -\gamma T_E \alpha \Delta T B_0 \qquad (1)$$

where α is the proportionality constant in the linear temperature dependence of σ_{tot} (Hindman 1966, De Poorter *et al* 1994, De Poorter 1995).

The sensitivity of the method is thus determined by α, by the echo time used in the pulse sequence and by the main magnetic field of the MRI scanner. It is evident that the method is also sensitive to changes in δB_0 between image acquisitions. Such changes may be due to drift of the external magnetic field, displacements of the object, or changes in magnetic susceptibility (De Poorter 1995, Ishihara *et al* 1995).

3. Materials and methods

3.1. Sample preparation and non-MR measurements

Samples were prepared for measurement of the temperature dependence of the proton resonance frequency shift in agarose gel, pure water, porcine liver and in the white of eggs. Furthermore, optically doped agarose gel samples were prepared, and the optical properties were measured.

3.1.1. Preparation of agarose gels. Nickel nitrate ($Ni(NO_3)_2{}^*6H_2O$, 1.55 g l^{-1}) was added to double-distilled water, forming a stock solution, where Ni^{2+} ions were used as a dopant in order to increase the signal-to-noise ratio by decreasing the T_1 relaxation time. A shorter T_1 relaxation time means that a larger fraction of the spin population will return to its original spin state during the repetition time, allowing the subsequent excitation to act on a larger magnetization. A comprehensive description of basic MRI is given by Woodward and Freimarck (1995). As compared with other paramagnetic dopants, such as Cu^{2+}, T_1 of Ni-doped phantoms depends very weakly on temperature (Kraft *et al* 1987). Two grams of agarose powder (type VI-A, Sigma-Aldrich, Sweden) was added to 100 ml of the Ni-doped water. The mixture was heated in a microwave oven (500 W), while occasionally stirred, until it boiled (approximately 1 min heating per 100 ml). Boiling was then allowed for about 1 min (without stirring) and evaporated water was replaced.

3.1.2. Preparation of liver tissue. In the first of two experiments on porcine liver, samples were taken from arbitrary parts of the liver, including the central parts where large blood vessels were present. The liver samples in the second experiment were selected after observation of gradient echo MR images of the entire liver, and regions that appeared inhomogeneous were avoided. In both experiments, the slice used for imaging was positioned where no air ducts were observed as spots with decreased signal. The egg whites, and the distilled water required no special preparation.

3.1.3. Preparation of an optically tissue-like MRI phantom material and measurement of optical properties. Agarose was dissolved in water according to the procedure described above. Polyvinylacetate microspheres (Mowilith 0530s, Hoechst, Perstorp, Sweden) with diameters between 1 and 6 μm (manufacturer's specification) were used to alter the

scattering coefficient, μ_s, and the anisotropy factor, g. The absorption coefficient, μ_a, was altered by addition of India ink (Higgins®, no 46030, Eberhard Faber Inc., Lewisburg, USA). The microspheres were delivered as a water dispersion (59% polyvinylacetate by weight) which was diluted with distilled water to a concentration of 30% by weight, in order to become less viscous and easier to dissolve. The microspheres were added to the agarose solution at temperatures below 75 °C. The ink was added at temperatures below 65 °C. Samples (without nickel nitrate) with microsphere concentrations ranging from 0.25 to 3.0% and with ink concentrations ranging from 0.25 to 2.5% were prepared for measurement of the optical properties. All samples were prepared from the same agarose solution by adding the optical dopants successively and by transferring a small amount of the mixture to a cuvette with a 1 mm thick cavity. Thus, the samples contained both microspheres and ink, assuming that the dopants acted as a nearly pure scatterer and a nearly pure absorber respectively. The error in the microsphere and ink concentrations due to the preparation procedure was estimated to be less than ±10%.

The optical properties of the gel samples were determined from measurements using an integrating sphere and a narrow-beam set-up. The equipment, as well as the calibration and measurement procedure, has been described previously by Nilsson *et al* (1995, 1998). Briefly, three parameters, the reflectance, the transmittance and the total attenuation coefficient (μ_t) were determined. The former two were obtained from the integrating sphere measurements and the latter from measurements in a narrow-beam geometry. The measured parameters were then linked to the optical interaction coefficients (μ_s, μ_a and g) through interpolation in a database established from Monte Carlo simulations (Nilsson *et al* 1998). The agreement between optical properties calculated from Mie theory and optical properties obtained from measurements on a suspension of polystyrene spheres, with certified particle size, followed by Monte Carlo interpolations has previously been verified in a series of calibration measurements (Nilsson *et al* 1995). From the results of the present measurements, five values (800–810 nm) were averaged for each sample in order to obtain the optical interaction coefficients at 805 nm, which was the specified wavelength of the laser used in this work. The optical interaction coefficients were plotted as a function of microsphere and ink concentration, and linear functions were fitted to the data points. Data on the scattering coefficient for microsphere concentrations above 0.75% were abandoned, since the narrow-beam set-up was not optimized for strongly scattering samples, leading to a slight influence of multiply scattered photons when the samples became more opaque.

3.2. MR measurements

All MR measurements were performed using a 1.5 T MRI scanner (Magnetom Vision, Siemens, Erlangen, Germany) and the standard head coil of the unit.

3.2.1. Assessment of the temperature coefficient of the proton resonance frequency. The relationship between phase angle change and temperature change was measured for 2% agarose gel ($n = 3$), pure water ($n = 1$), pig liver *in vitro* ($n = 2$) and in the white of eggs ($n = 1$). A spoiled gradient echo pulse sequence was used for image acquisition, with the following imaging parameters: repetition time (T_R) = 200–300 ms, echo time (T_E) = 15–20 ms, flip angle (FA) = 40°, number of signal averages (NSA) = 1, slice thickness = 10 mm, field of view (FOV) = 170 mm, matrix size = 128^2, scan time = 26–40 s.

The experimental set-up consisted of a Liebig condenser (no 115.610-400, Kebo, Stockholm, Sweden) connected to a circulating water bath (12 l) and four external reference

tubes used to correct for drift of the main magnetic field (figure 1). Temperatures were monitored by use of a fluoroptic thermometer (model 3000, Luxtron, Mountain View, CA, USA) with single-sensor probes. One probe was placed centrally in the test sample, contained in the central tube of the condenser, and one was placed where the circulating water entered the condenser. A third probe was placed in one of the reference tubes.

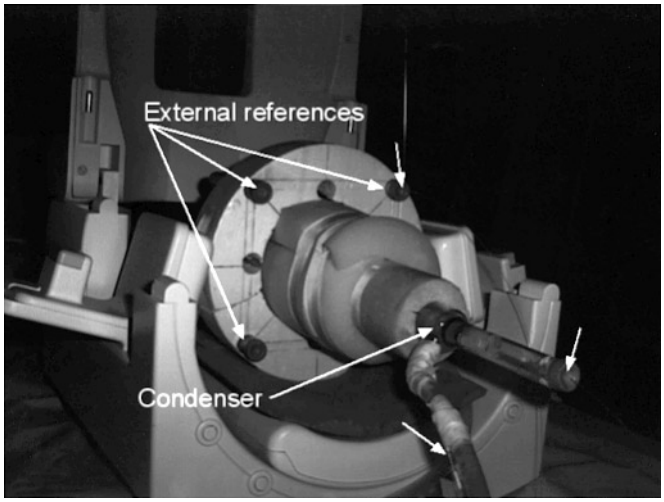

Figure 1. The experimental set-up used for the calibration measurements is shown. The central tube of the Liebig condenser contains the material that is examined. Four reference phantoms (only three are visible in the figure) containing Ni-doped agarose gel are used to monitor drift of the external magnetic field. Positions of the Luxtron fluoroptic probes are indicated by arrows.

Test samples in the condenser were heated and subsequently cooled by varying the temperature of the circulating water between 25 °C and 80 °C in steps of 5 °C. The water circulation was turned off during MR measurements. Each measurement was performed when the temperatures were the same in the test sample and in the water entering the condenser. A phase image obtained at 25 °C was used as a reference, and was subtracted from phase images acquired with other sample temperatures. The subtraction algorithm corrected for phase wrapping by addition or subtraction of 2π radians when the phase value after phase image subtraction was smaller than $-\pi$ or larger than $+\pi$, respectively (Ståhlberg *et al* 1989, De Poorter *et al* 1994). Phase changes ($\Delta\varphi$) in the resulting images were determined from a circular region of interest (ROI), with an area ≈ 0.65 cm^2, located centrally in the test sample. Phase changes in one of the reference tubes were subtracted to correct for drift of the main magnetic field. The other reference tubes served to check for spatial variations in the field drift. The slope ($\Delta\varphi/\Delta T$) was obtained by fitting linear functions to the data from heating and cooling respectively. Linear functions were also fitted to data points at temperatures between 25 and 45 °C. In each case the slope was used to calculate the temperature coefficient of the proton resonance frequency, i.e. α in equation (1). The magnetic flux density ($B_0 = 1.495$ T) was obtained from the actual resonance frequency of the MRI scanner.

3.2.2. Influence of optical dopants on MR images and relaxation times. The possible occurrence of artifacts in gradient echo images and/or changes in the relaxation times (T_1 and T_2) due to the optical dopants was examined. Two 250 ml rectangular bottles were

filled with 1.5% agarose gel containing only MR dopant (Ni^{2+}), and both MR and optical dopants (microspheres and ink) respectively. The Ni^{2+} concentration in the stock solution was 5.3 mM, which should result in a T_1 relaxation time of approximately 300 ms (Morgan and Nolle 1959). The use of agarose gel instead of an aqueous solution shortens T_2 but should not affect T_1 (Kraft *et al* 1987). The polyvinylacetate and ink concentrations were 4% and 1% respectively. A gradient echo MR image was acquired using $T_R/T_E = 500/20$ ms, FA $= 40^\circ$, NSA $= 1$, slice thickness $= 10$ mm, FOV $= 170$ mm, matrix size $= 256^2$, and scan time $= 128$ s. Also, MR images were acquired using spin echo pulse sequences with varying T_R and T_E ($T_R = 150$ and 600 ms, $T_E = 22.5$ and 45 ms), from which T_1 and T_2 images were calculated. The relaxation times were obtained as averaged pixel values within circular ROIs (area $= 5.5$ cm^2), positioned centrally in each phantom.

3.2.3. Measurement of temperature distributions during ILT. The accuracy and precision of the PRF method, when used for monitoring of the radial temperature distribution from a diffusing laser fibre (Lightstic, Rare Earth Medical, West Yarmouth, MA, USA), was evaluated in three experiments with varying echo times and scan times. The temperature distribution within a slice positioned along the laser fibre was registered in a fourth experiment.

Ni-doped (5.3 mM Ni^{2+}) agarose gel (1.5%) with 2% latex microspheres and 0.4% ink, corresponding to $\mu_s \approx 18$ mm^{-1}, $\mu_a \approx 0.17$ mm^{-1} and $g \approx 0.87$, was used. The optical properties were similar to those of native/coagulated porcine liver at 850 nm ($\mu_s = 10/45$ mm^{-1}, $\mu_a = 0.14/0.15$ mm^{-1} and $g = 0.96/0.94$) previously presented by Roggan *et al* (1995). The gel was moulded into a 500 ml cylindrically shaped plastic bottle (radius $= 35$ mm). A plastic template, holding the laser fibre and three fluoroptic probes at fixed positions, was contained in the bottle while the gel was moulded. The laser fibre had a 20 mm diffusing section with 1.45 mm outer diameter and was connected to a diode laser (Diomed 25, Diomed, Cambridge, UK) of 805 ± 25 nm wavelength. The radial distances between the temperature probes and the diffusing fibre, as defined by the template, were 5, 10 and 15 mm and coincided, to within ± 0.5 mm, with distances obtained from transverse MR images. The endpoints of the fluoroptic probes were positioned midway along the diffusing section of the laser fibre.

In all experiments, a reference MR image acquisition was started at time $(t) = -1$ min and another 30 images were acquired with 1 min intervals. The laser was turned on (distal power ≈ 2.2 W) at $t = 0$ min and was turned off at $t = 14$ min. The imaging parameters used in the first experiment were $T_R/T_E = 300/10$ ms, FA $= 68^\circ$, NSA $= 1$, slice thickness $= 5$ mm, FOV $= 110$ mm, matrix size $= 128^2$, scan time $= 40$ s. In the two subsequent experiments T_E was 20 ms while T_R was varied (30 ms and 300 ms) resulting in 6 s and 40 s scan time. The flip angle was calculated according to $\cos(\mathrm{FA}) = \exp(-T_R/T_1)$ (Chung *et al* 1996). Slices used for imaging were positioned orthogonally to the laser fibre and through the sensing points of the fluoroptic probes in the first three experiments. In the fourth experiment, when the imaging slice was aligned along the fibre, the imaging parameters were $T_R/T_E = 300/20$ ms, FA $= 68^\circ$, NSA $= 1$, slice thickness $= 5$ mm, FOV $= 140$ mm, matrix size $= 128^2$ and scan time $= 40$ s. Phase change images were calculated and subsequently transferred to MATLAB (Math Works, Natrick, MA, USA) for post-processing. In the first three experiments, ring-shaped ROIs were used to select pixels at radial distances of 5 ± 0.5, 10 ± 0.5 and 15 ± 0.5 mm, corresponding to the distances between the temperature probes and the laser fibre. Pixels at the positions of the actual probes were not selected. The point corresponding to the origin of the ROIs was chosen so

Table 1. The temperature dependence of the water proton resonance frequency, determined by fitting a linear function to measured phase changes in two temperature ranges (25–80 °C and 25–45 °C), are shown. For pig liver, linear fits were only obtained for temperature intervals where no marked deviations were present. R^2 is the square of the Pearson correlation coefficient.

Material	Expt no	Temperature coefficient (heating) (ppm °C^{-1})	R^2	Temperature coefficient (cooling) (ppm °C^{-1})	R^2
Agarose	1	0.0086 (25–75 °C)	0.9978	0.0087 (25-75 °C)	0.9994
Agarose	1	0.0092 (25–45 °C)	0.9993	0.0092 (25-45 °C)	0.9994
Agarose	2	0.0084 (25–80 °C)	0.9990	0.0088 (25–80 °C)	0.9943
Agarose	2	0.0092 (25–45 °C)	0.9992	0.0092 (25–45 °C)	0.9996
Agarose	3	0.0085 (25–80 °C)	0.9988	0.0082 (25–80 °C)	0.9974
Agarose	3	0.0094 (25–45 °C)	0.9996	0.0092 (25–45 °C)	0.9993
Pig liver	1	0.0080 (25–40 °C)	0.9985	—	—
Pig liver	2	—	—	0.0073 (25–80 °C)	0.9996
Pig liver	2	0.0079 (25–45 °C)	0.9976	0.0074 (25–45 °C)	0.9998
Egg white	1	0.0078 (22–80 °C)	0.9986	0.0076 (25–80 °C)	0.9988
Egg white	1	0.0086 (22–45 °C)	0.9991	0.0083 (25–45 °C)	0.9973
Water	1	0.0086 (25–80 °C)	0.9993	0.0084 (25–80 °C)	0.9974
Water	1	0.0089 (25–45 °C)	0.9995	0.0093 (25–45 °C)	1.0000

that the standard deviations of all pixel values within the ROIs were minimized. Temperature changes were obtained by insertion of the PRF temperature dependence (α) for agarose gel (25–45 °C), and the average phase changes ($\Delta\varphi$) for each ROI, into equation (1). When the scan time was 40 s, the nominal time point corresponding to each MR image was chosen to be the time at the start of the acquisition plus 20 s. The MRI derived temperatures at 5, 10 and 15 mm radial distances were plotted as a function of time, together with corresponding fluoroptic probe readings. In the first three experiments, standard deviations of pixel values ($n = 35$), belonging to the ROI at 5 mm distance from the laser fibre, were plotted as a function of time. In the fourth experiment, thermal images were calculated from MR measurements at 20 s, 4 min 20 s and 14 min 20 s.

4. Results

4.1. Assessment of the temperature coefficient of the proton resonance frequency

Measured temperature coefficients of the proton resonance frequency (ppm °C^{-1}) are shown in table 1. The PRF shift (ppm) versus temperature change (°C) during heating of Ni-doped agarose gel ($n = 3$) and distilled water ($n = 1$) is given in figure 2. An approximately linear relationship between temperature change and frequency shift over the entire temperature range was found for both agarose and water. The average temperature coefficients, in the 25–80 °C temperature range during heating, were 0.0085 ppm °C^{-1} and 0.0086 ppm °C^{-1} for Ni-doped agarose and water respectively. No hysteresis was observed between heating and cooling, but the temperature coefficient tended to be slightly smaller at

higher temperatures (table 1). The standard deviations of the measured phase angle changes corresponded to PRF shifts ranging from 0.001 to 0.002 ppm (Ni-doped gel) and from 0.002 to 0.014 ppm (water). The standard deviations for gel corresponded to temperature uncertainties ranging from ±0.14 °C to ±0.26 °C. As a rule, larger standard deviations were registered at higher temperatures.

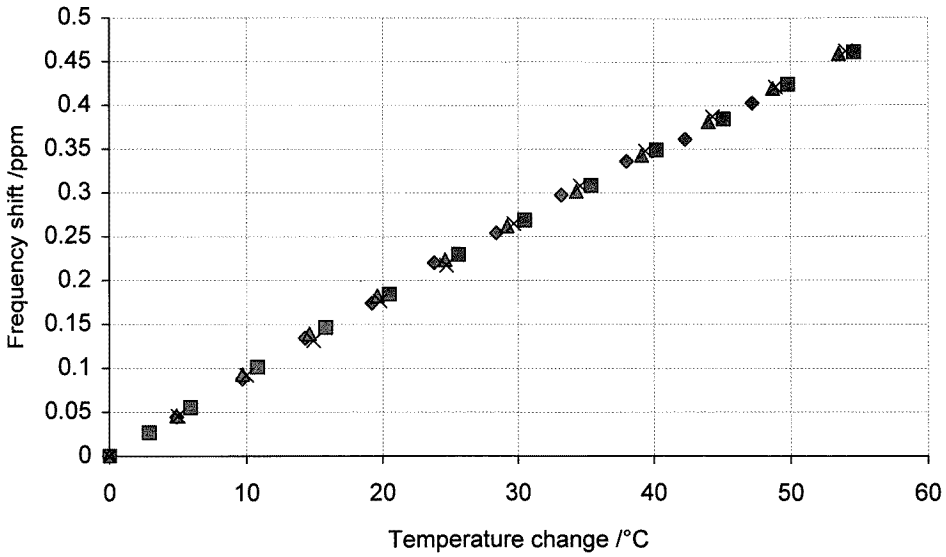

Figure 2. The temperature dependence of the water proton resonance frequency, as measured in the calibration experiments using three agarose preparations (◊, △, □) and pure water (×) is illustrated (heating only). A reference phase image, acquired when the sample temperature was close to 25 °C (corresponds to the origin in the figure), has been subtracted from all subsequent phase images. Correction for drift of the main magnetic field of the MR scanner was done. Temperature changes were obtained from fluoroptic probe measurements. Error bars corresponding to ±1 SD (not shown) were smaller than the markers.

Deviations from a linear relationship were observed in pig liver (figures 3(*a*) and 3(*b*)). In both experiments, phase angle changes appeared to increase linearly with temperature at temperatures below about 40 °C, with temperature coefficients of 0.0080 ppm $^{\circ}C^{-1}$ and 0.0079 ppm $^{\circ}C^{-1}$ in the first and second experiment respectively. In the second experiment, the deviation was not as prominent and a linear relationship was again found during cooling, but with the phase changes shifted towards values that were lower than during heating. The standard deviations of the phase changes for the second liver sample corresponded to PRF shifts ranging from 0.001 to 0.009 ppm (temperature changes ranging from 0.15 °C to 1.3 °C). For egg white, which also coagulated during heating, no marked deviation from a linear relationship was observed.

The corrections for non-temperature related phase changes were fairly small (<10 phase degrees, corresponding to a PRF shift of 0.022 ppm or a temperature change of approximately 2.4 °C) during the course of each experiment (at the most 4.5 h). During the first 30 min of each experiment the phase drift correction was never larger than four phase degrees (PRF shift = 0.0087 ppm corresponding to a temperature change of about 1 °C). Spatial variations were negligible.

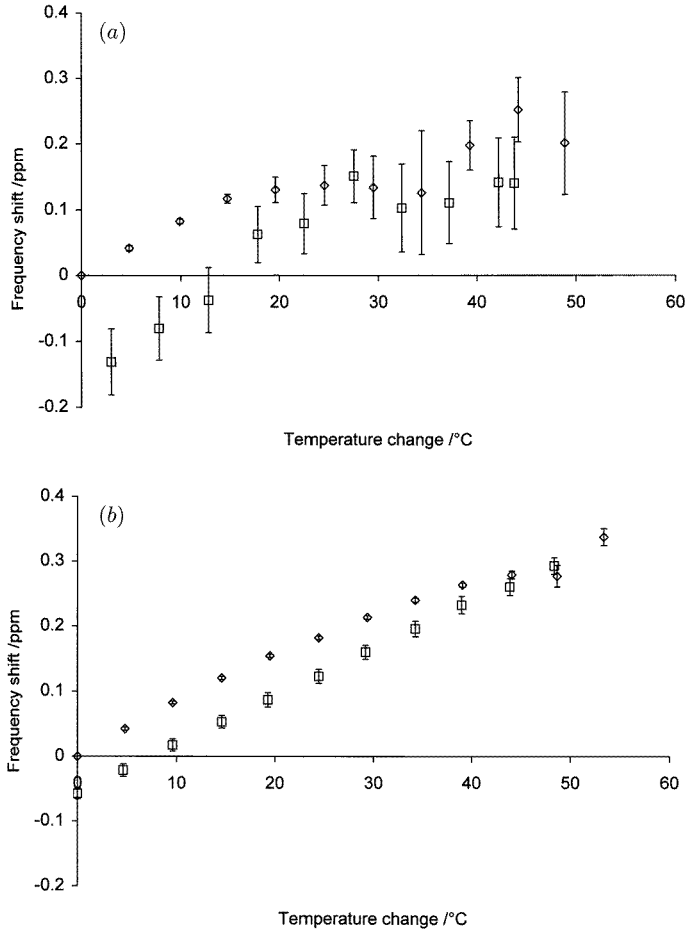

Figure 3. Proton resonance frequency shifts as a function of temperature change during heating (◊) and subsequent cooling (□) of pig liver samples showed deviations from a linear relationship. Smaller deviations were observed in the second experiment (*b*) as compared with the first experiment (*a*). Zero temperature change corresponds to 25 °C. Data points are averages, calculated from measured phase changes within a circular ROI placed centrally in the sample. The error bars correspond to ±1 SD.

4.2. Characterization of an optically tissue-like MRI phantom material

4.2.1. Optical properties. The results from the measurements of the optical properties of gel samples, with varying concentrations of latex microspheres and India ink, are shown in figures 4(*a*) and 4(*b*). The dependence of the scattering coefficient on the microsphere concentration was described by the linear relation $\mu_s = 8.7C + 0.52$ (mm^{-1}) where C is the concentration in g/100 g. The linear relation between the absorption coefficient and the ink concentration was $\mu_a = 0.43C - 0.004$ (mm^{-1}) where C is the concentration in ml ink per 100 ml gel mixture. A line, indicating the trend of any dependence of the anisotropy factor (g) on the microsphere and ink concentrations is also shown in the figures. The apparent increase of g values with increasing microsphere concentrations (figure 4(*a*)) was very uncertain ($R^2 = 0.05$), but there seemed to be a trend ($R^2 = 0.20$) of decreasing g

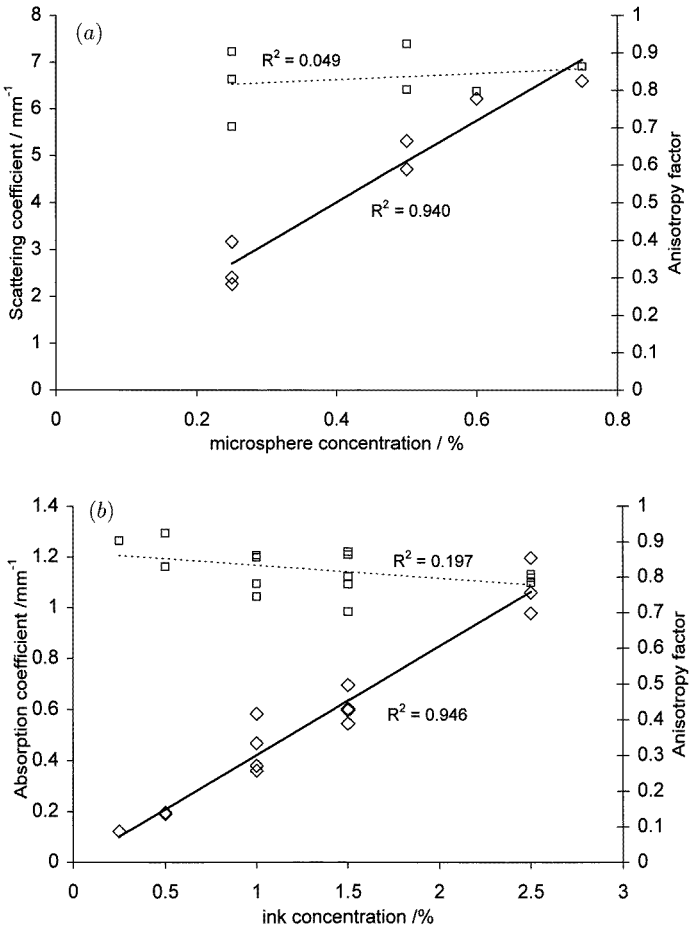

Figure 4. The scattering coefficient (◊) and anisotropy factor (□) for samples containing various concentrations of India ink and polyvinylacetate microspheres are shown as a function of microsphere concentration (*a*). Also, the absorption coefficient (◊) and anisotropy factor (□) are shown as a function of ink concentration (*b*). The squared Pearson's correlation coefficients (R^2), are shown in the graphs. Trendlines indicate a slight dependence of the anisotropy factor on ink concentration. All data were obtained at 805 nm wavelength.

values with increasing amounts of ink (figure 4(*b*)). The average g value, calculated from all measurements, was 0.82 ± 0.05 (mean $\pm$ 1 SD, $n = 15$). The g value originating from the microspheres and the agarose gel alone was estimated to 0.87 by extrapolation to zero ink concentration.

4.2.2. Influence of optical dopants on MR images and relaxation times. The relaxation times, T_1/T_2 (in ms), for Ni-doped gel with and without optical dopants was $281 \pm 4/65 \pm 3$ and $288 \pm 5/68 \pm 2$ respectively. Gradient echo images of the optically tissue-like phantom material appeared homogeneous and did not differ visually from images of agarose gel without optical dopants.

4.3. Temperature distributions during ILT

MRI derived temperatures and fluoroptic probe readings at 5, 10 and 15 mm radial distances from the laser fibre are shown as a function of time for the first experiment ($T_E = 10$ ms, scan time = 40 s) in figure 5. Figure 6 shows the standard deviations at 5 mm distance from the laser fibre for three experiments with varying echo times and scan times, including the experiment in figure 5. With $T_E = 10$ ms and 40 s scan time the random uncertainty ranged from 0.39 to 1.5 °C (1 SD). With $T_E = 20$ ms, random uncertainties ranged from 0.27 to 1.4 °C (1 SD) with 40 s scan time and from 0.82 to 1.8 °C (1 SD) with 6 s scan time. The smaller uncertainties were registered after the laser was turned off (see figure 6).

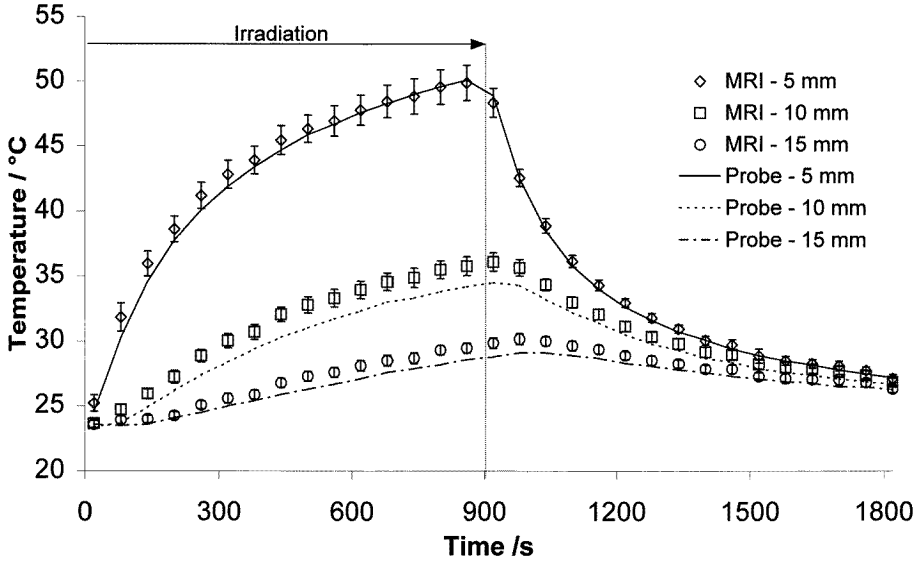

Figure 5. MRI derived temperatures as well as temperatures measured by fluoroptic probes are shown as a function of time during laser irradiation (15 min) in an optically tissue-like agarose gel, and during cooling after the laser was turned off. Ring-shaped ROIs were placed at 5, 10 and 15 mm radial distance from the laser fibre. The data points are averages of the calculated temperatures for all pixels within the ROI at that distance. Error bars correspond to ±1 SD.

Surface plots and corresponding contour plots of the temperature distribution from the fourth experiment are shown in figure 7. The images were acquired at $t = 20$ s, $t = 4$ min 20 s and $t = 14$ min 20 s. The contours clearly revealed the elliptical shape of the temperature distribution and the growth of the heated region with time. The surface plots showed some variation in temperature increase along the diffusing region of the laser fibre.

5. Discussion and conclusions

In this work, the PRF method was evaluated for use with tissue-like phantoms for interstitial laser thermotherapy. The phantom material should have thermal and optical properties similar to the tissue in question, and tissue *in vitro* might be the most obvious choice. However, tissue-mimicking phantoms have advantages as they could be made more homogeneous and well defined and since they may also be thermally reversible.

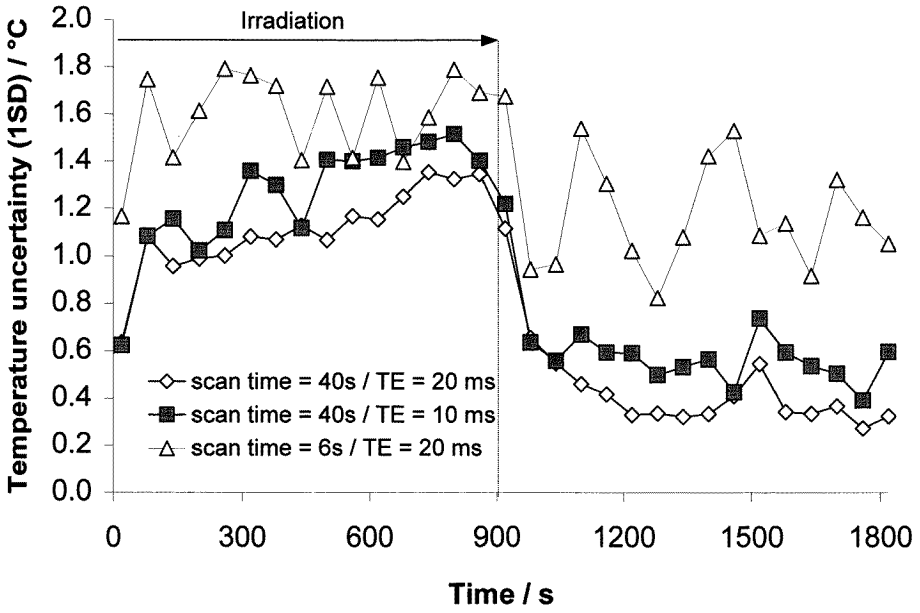

Figure 6. Uncertainties in the MRI derived temperatures (±1 SD) are shown as a function of time for three different laser irradiation (and cooling) sessions using agarose gel with optical properties similar to porcine liver. The uncertainties were generally larger during irradiation than during cooling. With 6 s scan time this effect was not as evident, due to the overall larger uncertainties. Smaller uncertainties were observed when more optimal imaging parameters were used ($T_E = 20$ ms, as compared with $T_E = 10$ ms).

Furthermore, the results from the experiments on porcine liver in the present study indicate that the use of tissue samples *in vitro* is not without problems. Contrary to what has been reported previously by Harth *et al* (1997), the calibration measurements on porcine liver resulted in deviations from a linear relationship between PRF shift and temperature change. The cause of this deviation is not entirely clear, but it may be related to tissue movements or structural changes during heating and subsequent coagulation. The measurements on egg white, which is quite homogeneous and also coagulates, indicate that the coagulation process itself does not cause severe deviations from a linear relationship. The large standard deviations are believed to be due to air present in vessels empty of blood, or gas bubbles formed during the heating process. Spots with low signal were readily visible in the modulus images during the first experiment on porcine liver, beginning at temperatures where deviations from a linear relationship started. In addition to selecting more homogeneous parts of the liver, as in the second experiment, the influence of air pockets could possibly be reduced by perfusing the tissue, for example with degassed saline, prior to the experiments. However, considering these difficulties in preparing useful tissue samples *in vitro*, it appeared reasonable to investigate the potential of a gel phantom as an alternative to tissue samples in ILT applications.

Agarose gel has often been used in MRI (Walker *et al* 1988, Kraft *et al* 1987) and has approximately the same thermal properties as water due to the high water content. In this respect the gel is also fairly similar to soft tissue, such as muscle and liver, with a water content between 70% and 85% (Duck 1990). The approximately linear relationship between PRF shift and temperature change shows that agarose gel is well suited for use with the

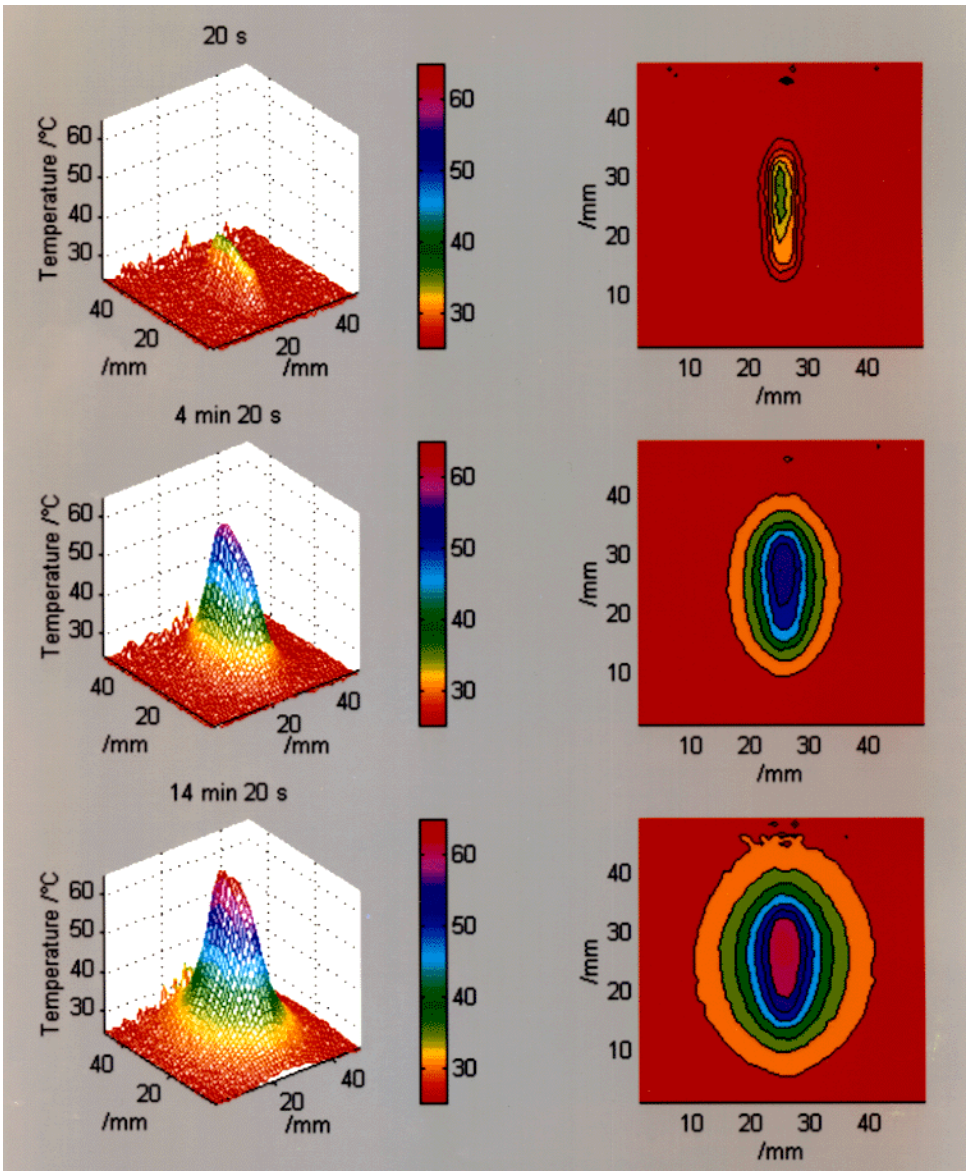

Figure 7. The temperature increase, as monitored with the PRF method, is shown at three different times during laser irradiation of optically tissue-like agarose gel. The contours correspond to temperature increases in steps of 2 °C (20 s) and 5 °C (4 min 20 s, 14 min 20 s) relative to a baseline temperature of 25 °C. The elliptical shape due to the 20 mm long diffusing section of the laser fibre is clearly visible.

PRF method in a wide temperature range. The measured temperature dependence of the proton resonance frequency in agarose gel (0.0085 ppm $^{\circ}C^{-1}$) was slightly smaller than previously reported for pure water (0.01 ppm $^{\circ}C^{-1}$) (Hindman 1966). However, calibration with pure water and agarose gel gave the same result in this study, which indicated that the gel behaves like water. There is some spread among previously reported temperature coefficients, but most *in vitro* studies show values of about 0.01 ppm $^{\circ}C^{-1}$. In the laser

irradiation experiments in this study, the deviations between MR-derived temperatures and probe readings would be smaller if a temperature coefficient of 0.01 ppm $^{\circ}C^{-1}$ was used, indicating a slight difference from the calibration measurements. This was not examined further, but Stollberger *et al* (1998) pointed out variations in the macroscopic magnetic field due to different temperature distributions and suggested corrections to be determined for each experimental set-up.

Regarding the optical properties, agarose gel is relatively transparent in the visible and near-infrared part of the electromagnetic spectrum, with a penetration depth of 18 mm at 700 nm (Duck 1990). Tissue is highly scattering and also somewhat absorbing (Cheong *et al* 1990, Roggan *et al* 1995). Polyvinylacetate microspheres and India ink appeared to be suitable to make the agarose gel optically tissue-like, and the wide range of scattering and absorption coefficients obtainable makes it possible to mimic several tissue types. The India ink acts to a small extent as a scatterer (Madsen *et al* 1992), which was reflected by the decreasing g value with increasing amounts of ink (more isotropic scattering). The rather large (0.52 mm^{-1}) scattering coefficient at zero microsphere concentration might be explained by the finite optical penetration depth in non-doped agarose gel, which appears somewhat 'milky', but could also in part be due to scattering particles in the ink. As proposed by Madsen *et al* (1992), this may be avoided by using molecular dyes, which should not act as scatterers, instead of ink. The offset at zero ink concentration was here close to zero, which indicated that the microspheres acted as pure scatterers. Contrary to Hushek *et al* (1993), who used $CuCl_2$ as a paramagnetic dopant, visually detectable inhomogeneity of optically doped gel samples was not observed in this study. Furthermore, no irreversible effects could be observed after the laser irradiation experiments.

It was demonstrated that the temperature distribution from laser fibres could be monitored with high accuracy and precision using the PRF method with the tissue-like phantom material presented in this work. The optimum imaging parameters with respect to the phase difference signal to noise ratio ($SNR_{\Delta\varphi}$) are specific for each tissue, and are determined for a gradient echo pulse sequence by the following conditions: $T_E = T_2^*$ and $\cos(FA) = \exp(-T_R/T_1)$ (Chung *et al* 1996). The first condition is found from optimization of T_E with respect to (i) the decrease in signal intensity with increasing loss of phase coherence and (ii) the phase-shift increase with increasing T_E (equation (1)). The second condition is the Ernst relation (Ernst and Anderson 1966). The effective transverse relaxation time (T_2^*) for the present phantom material was measured to be approximately 40 ms (data not shown), which implies that the $SNR_{\Delta\varphi}$ would be somewhat increased if $T_E = 40$ ms was used. The slightly smaller uncertainties using $T_E = 20$ ms as compared with $T_E = 10$ ms in this work, reflects the effect of using more optimal imaging parameters. A more marked increase of the random uncertainties was observed using 6 s scan time as compared to 40 s scan time. This may be an acceptable sacrifice if reasonably high temporal resolution is desired. Finally, a larger slice thickness increases the signal intensity and thus reduces the uncertainties, which is reflected by the smaller uncertainties in the calibration experiments (10 mm slice thickness) as compared with the laser fibre experiments (5 mm slice thickness). On the other hand, a larger slice thickness will cause larger partial volume effects (temperature variations within each voxel) that influence the accuracy of the temperature measurements. The smaller uncertainties observed when the laser was turned off may be due to reduced partial volume effects, as the temperature gradients were smaller during cooling than during irradiation. There is also a possibility of electromagnetic interference between the laser and the MR scanner, as the laser was not outside the scanner room. However, such interference could not be detected when images obtained with the laser switched on and off, respectively, were compared.

Non-invasive volumetric temperature imaging, using the PRF method in phantoms, provides a simple and efficient means to characterize different laser fibres with respect to their temperature distributions. Several types of diffusing fibres that distribute the laser light through a larger surface have been developed recently. Furthermore, multifibre systems may be used for ILT in order to increase treatment volumes (Ivarsson *et al* 1998). The use of diffusing fibres with multifibre systems will raise questions regarding, for example, the optimal fibre configuration for a certain target geometry, and numerical calculations can to some extent be used to answer such questions. However, MRI in combination with a tissue-like phantom material will be appropriate to assess effects of conditions that are not easily represented by mathematical models, such as asymmetric geometries or inhomogeneous (but well defined) media. Thermal or optical inhomogeneity may be represented in a gel phantom by inclusion of other materials, and complicated geometries may be obtained through moulding in several steps. The concept presented in this work would, for example, be directly applicable as a quality assurance tool in ILT.

It has been noticed that a possible disadvantage of agarose gels, as compared with polyacrylamide gels, would be the lower melting point (Hushek *et al* 1993). The gel used in this work has, however, a melting point of $95 \pm 1.5\,^{\circ}$C, which is close to the boiling point of water. This property might be useful to directly reveal temperature elevations at the fibre surface large enough to cause risk of evaporation and subsequent carbonization, which may be important to avoid during ILT (Möller *et al* 1996, Sturesson 1998).

It is concluded that agarose gel is well suited for use with the PRF method in a wide temperature range, and that polyvinylacetate microspheres and India ink are suitable to make the agarose gel optically tissue like. The present phantom material is advantageous for use in MRI applications since the optical properties and relaxation times may be altered independently, and since no image artifacts were observed. The temperature distribution from a diffusing laser fibre can be monitored with high accuracy and precision and non-invasive volumetric temperature imaging using the PRF method together with the proposed phantom material can be applied to assess effects of asymmetric geometries or inhomogeneous media. Considering the volumetric nature of MRI and the possibility of close to real time temperature monitoring, the present method is an alternative to thermistors or an infrared imaging camera, and offers several advantages.

Acknowledgments

This work was supported by grants from the Swedish Cancer Society (project no 95-1161), the Swedish Medical Research Council (project no K98-14P-12608-01A), Gunnar Arvid and Elisabeth Nilsson's Foundation for Cancer Treatment, Mrs Berta Kamprad's Foundation for Cancer Treatment, The Lund Health Care District's Research Foundations, The Royal Physiographic Society in Lund and John and Augusta Persson's Foundation for Scientific Medical Research.

References

Bown S G 1983 Phototherapy of tumours *World J. Surg.* **7** 700–9

Bolomey J and Hawley M 1990 *Non-Invasive Control of Hyperthermia (Clinical Thermology Subseries Thermotherapy: Methods of Hyperthermia Control)* ed M Gautherie (New York: Springer) pp 35–111

Cetas T C and Connor W G 1978 Thermometry considerations in localized hyperthermia *Med. Phys.* **5** 79–91

Cheong W F, Prahl S A and Welch A J 1990 A review of the optical properties of biological tissues *IEEE J. Quantum Electron.* **26** 2166–85

Chung A H, Hynynen K, Colucci V, Oshio K, Cline H E and Jolesz F A 1996 Optimization of spoiled gradient-echo phase imaging for *in vivo* localisation of a focused ultrasound beam *Magn. Reson. Med.* **36** 745–52

Clegg S T, Das S K, Zhang Y, Macfall J, Fallar E and Samulski T V 1995 Verification of a hyperthermia model method using MR thermometry *Int. J. Hyperth.* **11** 409–24

Cline H E, Hynynen K, Schneider E, Hardy C J, Maier S, Watkins R D and Jolesz F A 1996 Simultaneous magnetic resonance phase and magnitude temperature maps in muscle *Magn. Reson. Med.* **35** 309–15

De Poorter J 1995 Noninvasive MRI thermometry with the proton resonance frequency method: study of susceptibility effects *Magn. Reson. Med.* **34** 359–67

De Poorter J, De Wagter C, De Deene Y, Thomsen C, Ståhlberg F and Achten E 1994 The proton resonance frequency-shift method compared with molecular diffusion for quantitative measurement of two dimensional time dependent temperature distribution in a phantom *J. Magn. Reson.* **103** 234–41

Duck F A (ed) 1990 *Physical Properties of Tissue* (London: Academic)

Ernst R R and Anderson W A 1966 Application of Fourier transform spectroscopy to magnetic resonance *Rev. Sci. Instrum.* **37** 93–102

Firbank M, Oda M and Delpy D T 1995 An improved design for a stable and reproducible phantom material for use in near-infrared spectroscopy and imaging *Phys. Med. Biol.* **40** 955–61

Harth T, Kahn T, Rassek M, Schwabe B, Schwarzmaier H-J, Lewin J S and Mödder U 1997 Determination of laser-induced temperature distributions using echo shifted turbo FLASH *Magn. Reson. Med.* **38** 238–45

Hindman J C 1966 Proton resonance shift of water in the gas and liquid states *J. Chem. Phys.* **44** 4582–92

Hushek S G, Morrison P R, Kernahan G E, Fried M P and Jolesz F A 1993 Thermal contours from magnetic resonance images of laser irradiated gels *SPIE Proc.* **2082** 43–50

Ishihara Y, Calderon A, Watanabe H, Okamoto K, Suzuki Yo, Kuroda K and Suzuki Yu 1995 A precise and fast temperature mapping using water proton chemical shift *Magn. Reson. Med.* **34** 814–23

Ivarsson K, Olsrud J, Sturesson C, Möller P-H, Persson B R and Tranberg K-G 1998 Feedback interstitial diode laser (805 nm) thermotherapy system: ex vivo evaluation and mathematical modelling with one and four fibres *Lasers Surg. Med.* **22** 86–96

Jakob P M, Hendrich C, Breitling T, Schäfer A, Berden A and Haase A 1997 Real time monitoring of laser-induced thermal changes in cartilage *in vitro* by using snapshot FLASH *Magn. Reson. Med.* **37** 805–8

Jolesz F A, Bleier A R, Jakab P, Ruenzel P W, Huttl K and Jako G 1988 MR imaging of laser–tissue interactions *Radiology* **168** 249–53

Jolesz F A and Zientara G P 1995 MRI-guided laser-induced thermotherapy: basic principles *Laser Induced Interstitial Thermotherapy* ed G Müller and A Roggan (Washington, DC: SPIE Opt. Eng. Press) pp 294–324

Kraft K A, Fatouros P P, Clarke G D and Kishore P R S 1987 An MRI phantom material for quantitative relaxometry *Magn. Reson. Med.* **5** 555–62

Kuroda K, Miki Y, Nakagawa N, Tsutsumi S, Ishihara Y, Suzuki Y and Sato K 1991 Non-invasive temperature measurement by means of NMR parameters—use of proton chemical shift with spectral estimation technique *Med. Biol. Eng. Comput.* **29** 902

LeBihan D 1995 Temperature imaging by NMR *Diffusion and Perfusion Magnetic Resonance Imaging* ed D LeBihan (New York: Raven Press) pp 181–7

Madsen S J, Patterson M S and Wilson B C 1992 The use of india ink as an optical absorber in tissue-simulating phantoms *Phys. Med. Biol.* **37** 985–93

Marijnissen J P A and Star W M 1984 Phantom measurements for light dosimetry using isotropic and small aperture detectors *Porphyrin Localisation and Treatment of Tumors* (New York: Liss) pp 133–48

McKenzie A L 1990 Physics of thermal processes in laser–tissue interaction *Phys. Med. Biol.* **35** 1175–209

Möller P H, Hannesson P H, Ivarsson K, Olsrud J, Stenram U and Tranberg K-G 1997 Interstitial laser thermotherapy in pig liver: effect of inflow occlusion on extent of necrosis and ultrasound image *Hepato-Gastroenterology* **44** 1302–11

Möller P H, Lindberg L, Henriksson P H, Persson B R R and Tranberg K-G 1996 Temperature control and light penetration in a feedback laser thermotherapy system *Int. J. Hyperth.* **12** 49–63

Morgan L O and Nolle A W 1959 Proton spin relaxation in aqueous solutions of paramagnetic ions II. Cr^{+++}, Mn^{++}, Ni^{++}, Cu^{++}, Gd^{+++} *J. Chem. Phys.* **31** 365–8

Nilsson A M K, Berg R and Andersson-Engels S 1995 Measurements of the optical properties of tissue in conjunction with photodynamic therapy *Appl. Opt.* **34** 4609–19

Nilsson A M K, Sturesson C, Liu D L and Andersson-Engels S 1998 Changes in spectral shape of tissue optical properties in conjunction with laser-induced thermotherapy *Appl. Opt.* **37** 1256–67

Roggan A, Dörschel K, Minet O, Wolff D and Müller G 1995 The optical properties of biological tissue in the near infrared wavelength range—review and measurements *Laser-Induced Interstitial Thermotherapy* ed G Müller and A Roggan (Washington, DC: SPIE Opt. Eng. Press) pp 10–44

Roggan A and Müller G 1995 Dosimetry and computer-based irradiation planning for laser-induced interstitial thermotherapy (LITT) *Laser-Induced Interstitial Thermotherapy* ed G Müller and A Roggan (Washington, DC: SPIE Opt. Eng. Press) pp 114–56

Schneider W G, Bernstein H J and Pople J A 1958 Proton magnetic resonance chemical shift of free (gaseous) and associated (liquid) hydride molecules *J. Chem. Phys.* **28** 601–7

Ståhlberg F, Mogelvang J, Thomsen C, Nordell B, Stubgaard M, Ericsson A, Sperber G, Greitz D, Larsson H, Henriksen O and Persson B 1989 A method for quantification of flow velocities in blood and CSF using interleaved gradient-echo pulse sequences *Magn. Reson. Imaging* **7** 655–67

Stollberger R, Ascher P W, Huber D, Renhart W, Radner H and Ebner F 1998 Temperature monitoring of interstitial thermal tissue coagulation using MR phase images *J. Magn. Reson. Imaging* **8** 188–96

Sturesson C 1998 Interstitial laser induced thermotherapy: influence of carbonization on lesion size *Lasers Surg. Med.* **22** 51–7

Sturesson C and Andersson-Engels S 1995 A mathematical model for predicting the temperature distribution in laser-induced hyperthermia. Experimental evaluation and applications *Phys. Med. Biol.* **40** 2037–52

Sukowski U, Schubert F, Grosenick D and Rinneberg H 1996 Preparation of solid phantoms with defined scattering and absorption properties for optical tomography *Phys. Med. Biol.* **41** 1823–44

Vitkin A *et al* 1997 Magnetic resonance imaging of temperature changes during interstitial microwave heating: a phantom study *Med. Phys.* **24** 269–77

Wagnières G, Cheng S, Zellweger M, Utke N, Braichotte D, Ballini J-P and van den Bergh H 1997 An optical phantom with tissue-like properties in the visible for use in PDT and fluorescence spectroscopy *Phys. Med. Biol.* **42** 1415–26

Walker P, Lerski R A, Mathur-De Vré R, Binet J and Yane F 1988 Preparation of agarose gels as reference substances for NMR relaxation time measurement *Magn. Reson. Imaging* **6** 215–22

Woodward P and Freimarck R (eds)1995 *MRI for Technologists* (New York: McGraw-Hill)